Journal of Power Sources 657 (2025) 238224

Contents lists available at ScienceDirect

Journal of Power Sources

journal homepage: www.elsevier.com/locate/jpowsour

Towards selective Ir/IrO_2 electrochemical dissolution of Ir-based electrocatalysts for enhanced proton exchange membrane water electrolyzer sustainability

Jia Du [a,1], Matej Zlatar [b,c,1], Damin Zhang [a], Daniel Escalera-López [b], Jonathan Quinson [d,e], Serhiy Cherevko [b], Matthias Arenz [a,*]

[a] University of Bern, Department of Chemistry, Biochemistry and Pharmaceutical Sciences, Freiestrasse 3, 3012, Bern, Switzerland
[b] Helmholtz-Institute Erlangen-Nürnberg for Renewable Energy (IET-2), Forschungszentrum Jülich GmbH, 91058, Erlangen, Germany
[c] Department of Chemical and Biological Engineering, Friedrich-Alexander-Universität Erlangen-Nürnberg, Egerlandstr. 3, 91058, Erlangen, Germany
[d] Department of Chemistry, University of Copenhagen, Universitetsparken 5, 2100, Copenhagen Ø, Denmark
[e] Biological and Chemical Engineering Department, Aarhus University, 40 Åbogade, 8200, Aarhus, Denmark

HIGHLIGHTS

- Investigation of bifunctional Pt-Ir/C and Pt-IrO_2/C OER electrocatalysts.
- Treatment protocol influences the respective dissolution rates of Pt and Ir.
- Selective Ir dissolution in OER electrocatalysts.
- Proof-of-concept demonstration for Ir recycling.

ARTICLE INFO

Keywords:
Ir/IrO_2 dissolution
Pt dissolution IrO_2 recycling
Proton exchange membrane water electrolysis (PEMWE)
Proton exchange membrane fuel cells (PEMFC)

ABSTRACT

Electrocatalysts containing Ir are commonly used in energy conversion devices such as proton exchange membrane water electrolyzers (PEMWEs). However, the scarcity and high cost of Ir hinder their large-scale use. Therefore, there is a need for advanced Ir recycling schemes when scaling up PEMWE technology. Prior work on Pt-IrO_2/C nanocomposite catalysts indicates that IrO_2 has limited resistance to electrochemical degradation. Here, we built upon this observation to explore the selective dissolution of Ir/IrO_2 compared to Pt, using a scanning flow cell coupled to inductively coupled plasma mass spectrometry (SFC ICP-MS). We show that IrO_2 can even be selectively dissolved using a simple two-electrode setup. These findings are not only of fundamental interest for catalyst design but also highlight a potential pathway of electrochemically induced Ir recycling and regeneration strategies.

1. Introduction

One of the primary obstacles to the widespread commercialization of electrochemical energy conversion devices, such as proton exchange membrane water electrolysis (PEMWE) and proton exchange membrane fuel cells (PEMFCs), is the scarcity of the precious metals required to facilitate the electrochemical reactions [1–9]. Specifically, platinum (Pt) and iridium (Ir) are essential but limited resources, being among the rarest elements in the Earth's crust. The scarcity of these precious metals not only drives up their prices but also poses challenges to the scalability of the conversion devices. Several analyses have been published on the implications of limited Pt and Ir resources for PEMFC and PEMWE technologies, respectively [1–3,6]. While it is beyond the scope of this study to discuss this aspect in detail, a rough "back on the envelope" estimation reveals that considering an assumed requirement of 500 kg of Ir per GW and an annual Ir mining of approximately 4 tons, only 8 GW a^{-1} could be achieved – even if all mined Ir was allocated for PEMWEs, which is hardly a realistic scenario [1].

* Corresponding author.
E-mail address: matthias.arenz@unibe.ch (M. Arenz).
[1] Equally contributing first authors.

https://doi.org/10.1016/j.jpowsour.2025.238224
Received 1 July 2025; Received in revised form 15 August 2025; Accepted 22 August 2025
Available online 29 August 2025

Considering that to achieve renewable energy 'production and storage', often referred to as the "TeraWatt Challenge" [10], it becomes evident that the aforementioned estimations underscore the need for further advancements in catalysts for PEMWEs. However, equally significant is the urgent need to develop effective recycling schemes for precious metals. For instance, if implementing closed-loop Ir recycling by 2035, the PEMWE installed capacity in 2050 would increase by ~2.7x compared to that with no Ir recycling [11]. Platinum group metals (PGMs) are highly resistant to corrosion as well as electrically and thermally stable. Most literature concerning PGM recycling concentrates on Pt, Rh, and Pd, which are used in catalytic converters for cars [12]. The recycling schemes typically involve hydrometallurgical treatment of spent catalysts and focus on the leaching and separation of the individual elements [13]. For instance, certain recycling schemes involve the use of hot fuming *aqua regia* or pressurized alkaline cyanide solutions [14,15], which not only consume significant amounts of energy but are also harmful to the environment. Therefore, there is a need to improve in this area. Recently, an 'electrode-less' process platinum recycling scheme via induced surface potential alteration has been proposed [14]. Interestingly, in this concept, a so-called transient dissolution mechanism is exploited that is triggered by a repetitive change in platinum surface oxidation state via alternate purging with oxidizing and reducing gas. While the 'electrode-less' method mentioned above does not use external electric current or electrodes, the easiest way to introduce surface potential alteration is through electrochemical means. As for Ir, recycling schemes remain scarce, the state-of-the-art extraction methods for Ir are predominantly hydrometallurgical processes, which are typically carried out at high temperatures using harsh chemicals, e.g., *aqua regia* [16], tetrafluorobromate [17], etc. In these processes, the leaching/dissolution of Ir generally constitutes the rate-determining step [18]. Only recently, Ir dissolution by electrochemical means has been proposed [19].

Here we follow this recently suggested route and explore the potential of selective Ir electrochemical dissolution from Pt-Ir/Pt-IrO_2 bifunctional electrocatalysts. The focus and scope of this work is on providing a proof-of-concept demonstration of selective Ir dissolution via electrochemical methods, rather than evaluating the subsequent Ir recovery. As a model system for an electrocatalyst, we employed nanocomposites [20,21], which combine different nanoparticles (Pt and IrO_2/Ir) on the same carbon support material. Previously, such catalysts have been prepared as bifunctional Pt-IrO_2/Pt-Ir catalysts, but they demonstrated limited electrochemical stability of IrO_2 during repetitive changes in the electrode potential [20,22,23]. Following this observation, we studied the model nanocomposite catalysts to demonstrate the selective dissolution of IrO_2/Ir, which could serve as a conceptual framework for an electrochemical Ir recycling strategy. We tested the principle using scanning flow cell measurements coupled with inductively coupled plasma mass spectrometry (SFC-ICP-MS) [24]. This approach allows us to monitor online metal dissolution as a function of the applied electrode potential, making it ideal for evaluating various electrochemical treatment protocols. It has been reported that when Pt-IrO_2 bifunctional catalysts are used at a reversal-tolerant anode for PEMFC, the H_2 gas at the anode with elevated temperature (80 °C) can chemically reduce a few outer monolayers of the surface of IrO_2 nanoparticles to metallic Ir, which then is more prone to dissolution [25]. Thus, to distinguish between two pathways of Ir dissolution – via a reduction of IrO_2 to Ir under a hydrogen atmosphere [25] and direct IrO_2 dissolution – we tested inert atmosphere and air conditions, as well as metallic Ir and IrO_2 nanoparticles.

2. Experimental

2.1. Synthesis of supported metallic Pt and nanocomposite

The synthesis methods for supported catalysts are detailed in previous studies [20,26], which includes the microwave-assisted preparation of metal (Pt and Ir) NPs and the post-immobilization of metal NPs onto carbon support (Vulcan XC72R). Monometallic Pt NP solution, or Pt and Ir NP solutions, were simultaneously added to carbon suspension to differentiate the obtained catalyst was supported monometallic or nanocomposite catalysts. The content of Pt and Ir NPs was kept 20 % in weight (wt.%) throughout the prepared supported catalysts.

2.2. Transmission electron microscopy (TEM)

TEM was used for physical characterization of the as-prepared catalysts. A Jeol 2100 transmission electron microscope operated at 200 kV was used for TEM analysis. The catalyst dispersion diluted in ethanol was dropped on carbon coated copper TEM grids (Quantifoil) for TEM sample preparation. Images were recorded at least three randomly selected areas. The representative TEM micrographs of the studied catalysts are displayed in Fig. S1.

2.3. Small angle X-ray scattering (SAXS)

The size distributions of the studied catalysts were evaluated by SAXS and shown in Fig. S1. SAXS measurements and data analysis were performed as detailed in the previous study [21]. The scattering data are fitted to the expression:

$$I(q) = A \cdot q^{-n} + C \cdot \int P(q,R)V(R)D(R)dR$$

Where $A \cdot q^{-n}$ is the power law in which A and n are free parameters, C is a scaling constant, P is a sphere form factor, V is the particle volume, and D the log-normal size distribution, and the scattering vector $q = 4\pi \cdot \sin(\theta)/\lambda$, The sphere form factor is expressed as:

$$P_s(q,R) = \left(3\frac{\sin(qR) - qR\cos(qR)}{(qR)^3}\right)^2$$

and the log-normal distribution is expressed as:

$$D(R) = \frac{1}{R\sigma\sqrt{2\pi}} e^{\left(\frac{-\left[\ln\left(\frac{R}{R_0}\right)\right]^2}{2\sigma^2}\right)}$$

The fitting was conducted with a home written MATLAB code. The values obtained for free parameters in the model are listed in Table S1, note that the data from 20 wt% Pt were already previously reported [21] and shown here to compare with 20 wt% Pt + 20 wt% Ir (Pt-Ir/C).

In our previous work [21] using 20 wt% Pt and 40 wt% Ir, the SAXS data were best fitted using two size populations. However the size of the Pt and Ir nanoparticles are so closed that in the case of less scattering material for a 20 wt% Pt and 20 wt% Ir, a single size model is enough to fit the data and the mean retrieved size is around 2 nm, in agreement with the expected size of the Pt and Ir nanoparticles and the rather homogenous size of the nanoparticles observed by TEM on this sample.

2.4. Scanning electron microscope (SEM)-based energy dispersive X-ray spectroscopy (EDX)

The compositions of nanocomposites before and after treatments were evaluated with SEM-EDX. An equipment of Zeiss Gemini 450 SEM coupled with an Oxford Instruments UltimMax 65 EDX detector was used and a voltage of 25 kV was applied for analysis. Before treatment, a Ø 3 mm of pre-filtered catalyst layer was punched and fixed on top of a sticky carbon tape, which was placed on the metallic sample holder. The catalyst layer after composition analysis served as working electrode and used for electrochemical treatment. Afterwards, the Ø 3 mm catalyst layer was transferred again to SEM-EDX to determine the change of relative Pt/Ir weight ratio during electrochemical treatment. Five

independent spots of a catalyst layer were selected for analysis for each studied sample.

2.5. Inductively coupled plasma mass spectrometry (ICP-MS)

The contents of the dissolved Pt and Ir in electrolyte after jacketed-based electrochemical treatment were evaluated with ICP-MS (NexION 2000 ICP-MS). The ICP-MS was equipped with a cyclonic spray chamber and a PFA-nebulizer. 5 mL of electrolyte in cell after electrochemical treatment was taken and diluted with Milli-Q water to an ideal concentration for further ICP-MS analysis.

2.6. Scanning flow cell with inductively coupled plasma mass spectrometry (SFC-ICP-MS)

The outlet of scanning flow cell (SFC) was coupled with inductively coupled plasma mass spectrometry (ICP-MS) to detect dissolved metal ions during the applied electrochemical protocol. An Ar-purged 0.05 M H_2SO_4 electrolyte was prepared by diluting concentrated H_2SO_4 (Suprapure 96 %, Merck) with ultrapure water and then circulated through the SFC. Before entering the ICP-MS, an internal standard was introduced at a 1:1 mixing ratio using an ICP-MS peristaltic pump, with a flow rate of approximately 3.5 μL/s. The counter electrode (graphite rod, 5 mm, HTW Sigradur G) and reference electrode (Ag/AgCl, Metrohm, Germany) were positioned at the SFC inlet and outlet. The working electrodes were prepared by drop-casting method onto glassy carbon (5 × 5 cm, Sigradur G, HTW) backing electrode and approached from above with an XYZ position stage. All the electrodes were connected to a Gamry Reference 600 potentiostat (Gamry Instruments), while the potentials were calibrated against the RHE scale. ICP-MS instruments, PerkinElmer NexION 350X and 300X, were calibrated using 3-point calibration with solutions of investigated elements. Internal standard solutions were used to monitor potential instrument drifts and matrix effects. Further details can be found in our previous publications.

2.7. Preparation of working electrodes for SFC-ICP-MS measurements

The working electrodes were prepared by dispersing the powder in a 7:1 ratio of H_2O (Merck, Mili-Q IQ 7000, 18 MΩ, total organic carbon < (TOC) < 3 ppb) and isopropanol (Emsure®, Merck, ≥99.8 % purity). To prevent catalyst detachment, Nafion ionomer solution (D-520, Sigma Aldrich, 5 wt %) was used as a binder at a catalyst-to-ionomer weight ratio of 4:1. The mixture underwent 15 min of sonication in an ice bath using a horn sonicator (Branson Ultrasonics SFX150) with 4 s on/2 s off pulses. Following sonication, the pH was adjusted to around 11 using 1 M KOH before drop-casting a 0.2 μL suspension (0.66 mg/mL) onto glassy carbon (GC) substrates (5 × 5 cm^2, Sigradur G, HTW). The estimated catalyst loading of approximately 10 μg cm^{-2} depended on the size of the catalyst ink spots, as evaluated using a Keyence VK-X250 profilometer.

2.8. Preparation of working electrodes for jacket-type cell measurements

The catalyst layer (nominal loading of 200 $\mu g_{Pt/Ir}\ cm^{-2}_{geo}$) was fabricated via vacuum filtration, which was detailed elsewhere [27]. Afterwards, a rectangular carbon-based GDL (1 cm × 3 cm, with MPL on the top) was applied for WE fixing, in which, a Ø 3 mm of the pre-filtered catalyst layer was punched and placed on top of the rectangular GDL, which was further fixed with Teflon tape to ensure that the Ø 3 mm WE was stabilized and exposed to electrochemical treatments.

2.9. Electrochemical measurements in a jacket-type cell

All electrochemical treatments based on the more realistic catalyst loading 400 $\mu g_{Ir\ +\ Pt}\ cm^{-2}_{geo}$, i.e. 1000-1200 $\mu g_{Cat.}\ cm^{-2}_{geo}$) were performed in a three-electrode system connected with a potentiostat (ECi-200, Nordic Electrochemistry ApS), which was controlled by a computer. A jacket-type electrochemical cell with a hollow outer layer for water circulation for temperature controlling, was used for electrochemical treatments. A carbon rod was used as counter electrode (CE), the WE was detailed in the last section. All potentials were determined with respect to RHE, which was prepared prior to each measurement. Electrochemical measurements were conducted in air at 40 °C, maintained by circulating water through the outer layer of the jacket-type cell. After reaching the set temperature, an additional 10 min equilibration period was allowed to ensure the electrolyte within the inner compartment attained the target temperature. The electrolyte was stirred using a magnetic stirrer during measurements. Different electrolyte (1 M H_2SO_4, 1 M $HClO_4$, 1 M HNO_3 and 1 M H_2SO_4 + 0.5 M CH_3OH) was used for electrochemical treatments. The following procedures were implemented sequentially in treatments: catalyst surface cleaning, catalyst oxidation/activation (only for nanocomposite) and degradation. For supported monometallic Pt/C, continuously swept potential between 0.05 and 1.10 V vs RHE at a scan rate of 500 mV s^{-1} served as a typical protocol for catalyst surface cleaning, ~30 repeats were performed to obtain a stable cyclic voltammograms. For supported Pt-Ir/C nanocomposite, potentials were swept in a limited window of 0.10 V–0.30 V vs RHE with a scanning speed of 100 mV s^{-1} for ~20 cycles, during which the solution resistance was compensated to between 2 and 3 Ω via an analog positive feedback scheme. An additional catalyst electrochemical oxidation/activation procedure by holding potential at 1.60 V vs RHE for 8 min was needed for Pt-Ir/C nanocomposites to form IrO_2. Afterwards, potential was cycled between 0.05 and 1.10 V vs RHE at a scan rate of 500 mV s^{-1} to obtain stable cyclic voltammograms. Concerning degradation test, a current control mode was employed, in which, the applied current was stepped between −1 mA cm^{-2} and 1 mA cm^{-2} with a rest time of 1 s at each current, the total treatment lasted for 1 h. After electrochemical treatments, 5 mL of electrolyte was preserved for ICP-MS analysis.

3. Results and discussion

3.1. Impact of measurement protocols on the dissolution rates of Pt and Ir from Pt-Ir/C catalysts

We begin our discussion by comparing the metal dissolution of two catalyst types: a standard Pt/C catalyst and a Pt-Ir/C nanocomposite catalyst. Both catalysts have a fixed Pt metal loading, i.e., 20 wt%, and similar particle sizes of Pt and Ir [20], as shown in Fig. S1 and Table S1. As mentioned in the introduction, to analyze the metal dissolution, we investigated thin catalyst films prepared by the drop-casting method in SFC-ICP-MS measurements [24].

For the first protocol, we choose a mild approach by applying potential steps between 0.80 and 1.10 V vs. reversible hydrogen electrode (RHE). This potential range simulates the cathode operation of PEMFCs under standard conditions. By selecting this range, our aim was to prevent the complete oxidation of Ir and the formation of an IrO_2 phase [28,29]. Fig. 1 illustrates the initial dissolution of the metal upon establishing potential contact, primarily driven by the reduction of the native metal oxide formed due to catalyst exposure to air [30]. Interestingly, in the bifunctional Pt-Ir/C catalyst, the dissolution of Ir is significantly more pronounced compared to Pt. This finding can be attributed to the higher tendency for Ir to form oxide species in air, which are reduced upon establishing potential contact [30]. However, once the degradation protocol begins, both Ir and Pt dissolution occur at similar rates in the Pt-Ir/C catalyst. This finding suggests that an electrochemical recycling scheme based on such a protocol would require the separation of the individual elements after their dissolution. Nevertheless, in comparison to the standard Pt/C catalyst, the presence of Ir in the Pt-Ir/C catalyst inhibits Pt dissolution and bifunctional Pt-Ir/C catalysts can effectively mitigate the dissolution of the active Pt catalyst.

In a second protocol that was tested to identify conditions for

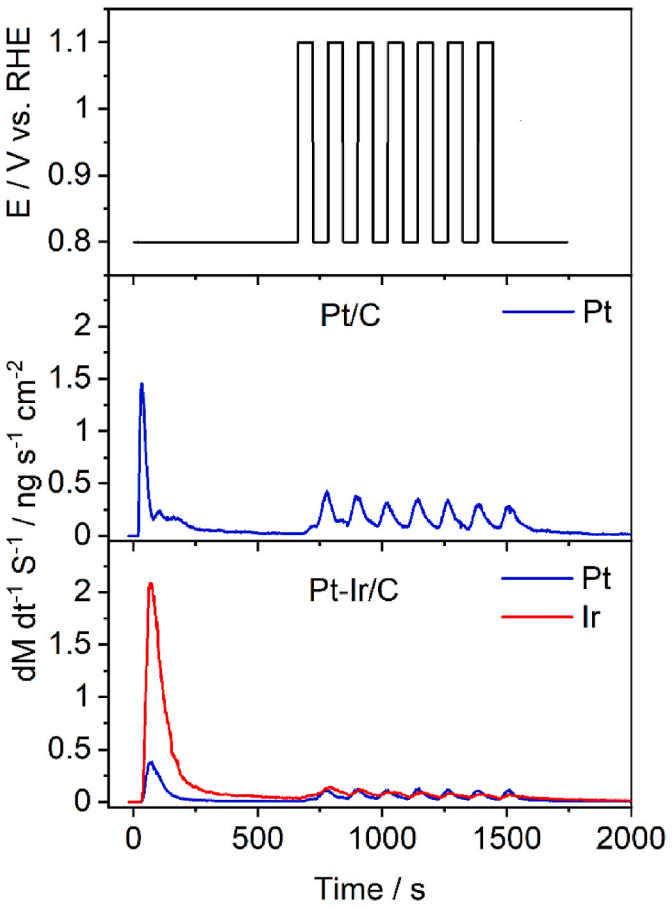

Fig. 1. Mass-specific metal dissolution rates of 20 wt% Pt/C (Pt/C, in the middle) and 20 wt% Pt + 20 wt% Ir/C (Pt-Ir/C, on the bottom). The applied treatment protocols are plotted at the same time scale as metal dissolutions. The applied potential steps between 0.80 and 1.10 V vs RHE with a rest time of 60 s on each and repeats for 7 times in total.

selective metal dissolution, the upper potential limit was adjusted from 1.10 V to 0.90 V vs RHE. As depicted in Fig. 2a, this modification in the protocol results in a reduction of Pt dissolution, while the dissolution of Ir remains unchanged as compared to that in Fig. 1. This finding aligns with a previous study that indicated the onset dissolution potentials of 0.85 V vs RHE for Ir and 0.95 V vs RHE for Pt, respectively [31]. However, altering the lower potential limit in the degradation protocol (lower voltage reached) from 0.80 to 0.05 V vs RHE has a significant influence on the dissolution of Ir, as illustrated in Fig. 2b, while it has a negligible impact on Pt dissolution. This suggests that the kinetic acceleration of Ir oxide reduction at low potentials leads to its substantial cathodic dissolution [28,32,33].

Our findings can be compared with previous studies of Pt-Ir/C bifunctional catalysts [23,25] which were performed with a focus on the activity and stability of the catalyst, not its selective dissolution. The work indicated significant performance limitations due to the dissolution of metallic Ir even at upper potential limits that were well below those experienced during abnormal operations of PEMFCs, such as hydrogen depletion conditions [34,35] and repeated start-up/shutdown cycles [36].

3.2. Investigation of Ir dissolution from Pt-IrO_2/C catalysts

In another study [25], it was proposed that the reduction of IrO_2 to Ir plays a crucial role in Ir dissolution within the hydrogen atmosphere of a PEMFC anode. Consequently, we aimed to investigate whether the type of protocol proposed (e.g. shown in Fig. 2) is limited only to metallic Ir or if IrO_2 is also susceptible to selective dissolution. To accomplish this, prior to the dissolution measurements we subjected the Pt-Ir/C catalyst to full activation (i.e., oxidation, see Experimental section for further details), creating a Pt-IrO_2/C nanocomposite that is active for the OER [20,37,38]. We then subjected this composite to a treatment designed to trigger selective Ir dissolution. The results presented in Fig. 3 indicate that Ir dissolution is not confined to metallic Ir formed in a reductive hydrogen atmosphere. Significant Ir dissolution occurs regardless of whether Ir or IrO_2 is present in the catalyst. As described before, the introduction of Ir to Pt/C to form a bifunctional catalyst can protect the Pt catalyst and carbon support, but this protection comes at the cost of substantial Ir dissolution.

3.3. Underlying Ir/Pt dissolution mechanisms

The dissolution observed in this study follows three well-established pathways for Ir [28,29,39], Pt [40–42], and other noble metals [30,32]. The first pathway emerges immediately upon contact with the electrolyte, marked by dissolution peaks associated with the reduction and/or chemical dissolution of native oxides formed during air exposure (Figs. 1–3), as discussed by Cherevko et al. [30]. In our measurements, Ir consistently exhibits larger initial peaks than Pt, suggesting the presence of thicker native oxides. The subsequent reduction of these oxides promotes greater cathodic and/or chemical dissolution, consistent with earlier observations.

A second pathway becomes active during potential transitions, where transient dissolution can occur through the loss of short-lived oxide or hydroxide species, direct electrochemical dissolution of the metal or its oxide [43], or via the place-exchange mechanism [44–47]. The latter initiates once a critical oxygen coverage is reached, producing soluble Ir^{3+} or Pt^{2+} prior to continuous oxide growth. Based on Pourbaix diagrams, neglecting kinetic and mass-transport effects, the thermodynamically favoured anodic reactions are:

For Ir: $Ir \rightarrow Ir^{3+} + 3e^-$

$Ir + 2H_2O \rightarrow IrO_2 + 4H^+ + 4e^-$

For Pt: $Pt \rightarrow Pt^{2+} + 2e^-$

$Pt + H_2O \rightarrow PtO + 2H^+ + 2e^-$

$Pt + 2H_2O \rightarrow PtO_2 + 4H^+ + 4e^-$

Nernst-derived anodic dissolution “onset potentials” at 1 nM (estimated for SFC-ICP-MS measurements) are 0.98 V vs RHE for Ir (0.82 V vs RHE in other reports) and 0.92 V vs RHE for Pt, while experimental “onset potentials” of 0.85 and 0.95 V vs RHE have been reported [48]. These distinct thresholds enable selective tuning of the dissolution behaviour. In Pt-only samples pulsed between 0.8 and 1.1 V vs RHE (Fig. 1, middle), anodic dissolution via Pt–O place exchange predominates, competing with passivation, whereas cathodic transient dissolution exceeds the anodic contribution only when the upper limit surpasses 1.1 V vs RHE [40] or the lower limit falls below 0.8 V vs RHE [41].

In Pt–Ir nanocomposites (Fig. 1, bottom), pulsing between 0.8 and 1.1 V vs RHE suppresses Pt dissolution relative to Pt-only samples. Lowering the upper limit to 0.9 V vs RHE decreases Pt dissolution while leaving Ir largely unaffected (Fig. 2a), a trend reflecting Pt’s higher oxide-formation potential, which limits oxide growth and subsequent reduction at 0.8 V vs RHE, thereby reducing cathodic dissolution. In a complementary protocol (Fig. 2b), Pt dissolution is completely eliminated, while, as in the previous case, Ir dissolution remains unchanged. For Ir, most dissolution occurs during the low-potential hold due to reduction of oxide formed during the preceding anodic step, whereas for Pt, the potential is insufficient to form such oxides. The strong dependence of cathodic dissolution on the lower potential limit, and its correlation with oxide coverage, aligns with earlier studies [33,41].

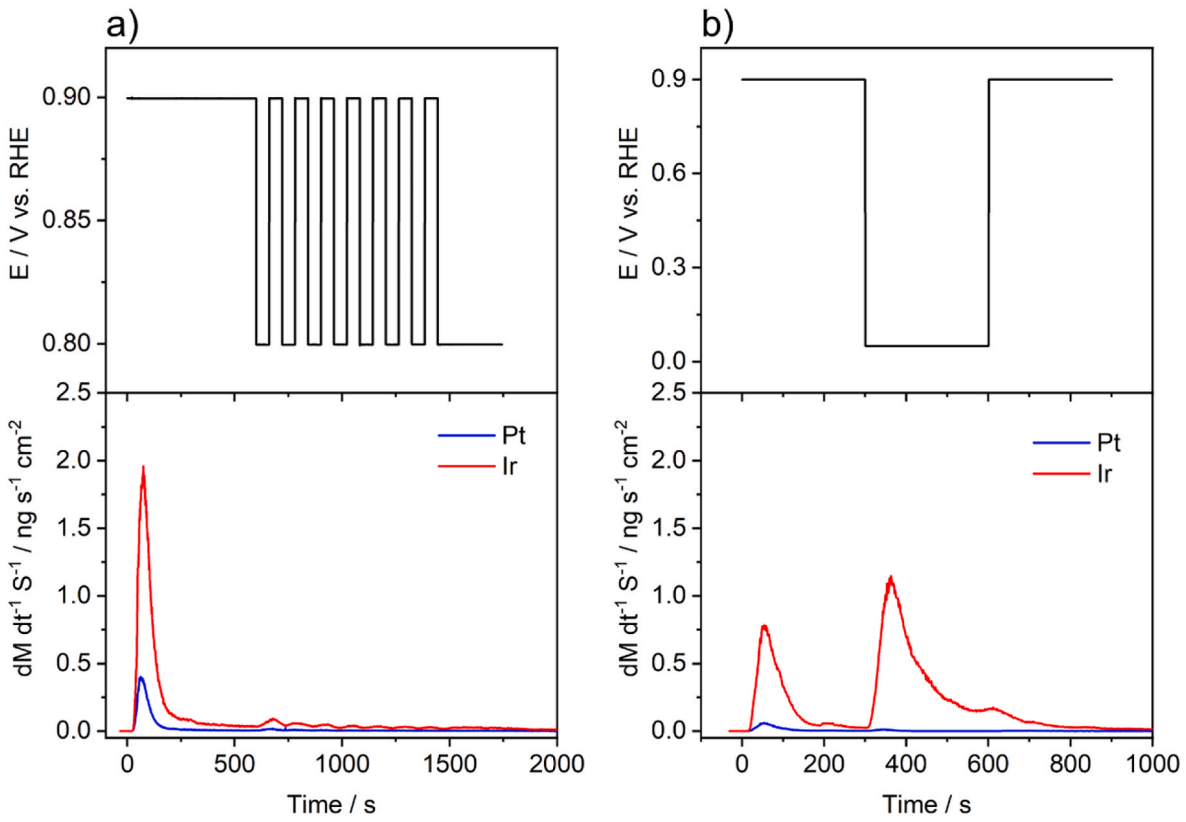

Fig. 2. Mass-specific metal dissolution rates of Ir (red curve) and Pt (blue curve) of 20 wt% Pt + 20 wt% Ir/C (Pt-Ir/C) nanocomposite exposed to different treatments for (a) the applied potential steps between 0.90 and 0.80 V vs RHE with 60 s resting on each and repeats for 7 times and (b) the applied potential steps between 0.90 and 0.05 V vs RHE with 300 s resting on each potential. (For interpretation of the references to colour in this figure legend, the reader is referred to the Web version of this article.)

The third pathway becomes dominant under OER-relevant, transpassive conditions [28,32,43], where Ir can further oxidize to Ir^{5+} / Ir^{6+}, and dissolution likely shares intermediates with the OER [49]. As shown in Fig. 3, Ir, owing to its lower OER overpotential in acid [32,43,50], facilitates both oxygen evolution and associated dissolution, whereas Pt remains largely inactive or passivated. Under these conditions, dissolution arises from combined contributions of transient anodic dissolution and steady-state dissolution coupled to the OER. Ir oxides formed during OER also promote cathodic transient dissolution in subsequent galvanostatic pulses. Over time, incomplete oxide reduction leads to progressive surface passivation [28], shifting the system from a mixed transient/steady-state regime to a predominantly steady-state dissolution mode.

3.4. *Envisioning Ir electrochemical recycling via its selective dissolution*

The results depicted in Figs. 2b and 3, however, unveil a fascinating aspect of Ir dissolution selectivity, which we envision to be exploitable in an electrochemical recycling scheme. Notably, when the potentials are varied between 0.90 and 0.05 V vs RHE, a selectivity in Ir dissolution of approximately 25 % is achieved, while Pt dissolution remains below 0.5 % for the Pt-Ir/C bifunctional catalyst, see Fig. 4. Furthermore, by employing a protocol that alternates the electrode current between +1 mA cm^{-2} and -1 mA cm^{-2} (corresponds to a potential pulse ranging from approximately 0 V–2 V vs RHE) the relative amount of dissolved Ir in comparison to dissolved Pt is significantly higher for the Pt-IrO_2/C catalyst, see Fig. 3. During the current pulse, Ir dissolution is approximately 30 times higher than Pt dissolution (approximately 30 % Ir and 0.8 % Pt dissolution), and it is even possible to selectively dissolve almost all Ir (96 %) from the Pt-IrO_2/C catalyst throughout the entire protocol, as detailed in Fig. 4.

In other words, in both cases, the potential excursions result in nearly exclusive Ir dissolution, while the Pt remains relatively stable. Although this phenomenon does not alleviate the limitations of bifunctional catalysts in mitigating the carbon oxidation reaction (COR) during abnormal PEMFC operations, it suggests the potential development of a low temperature electrochemical pathway for Ir recycling from bifunctional catalysts, capitalizing on the observed selectivity. Ir recycling is a crucial process for reusing Ir-containing electrocatalysts [51]. Particularly for bifunctional Pt-Ir/Pt-IrO_2 catalyst layers, the first step involves removing the precious metals from the catalyst layer and subsequently selectively recovering them. If selective removal from the catalyst layer can be achieved, the selective recovery of Ir and Pt would not be necessary.

However, for an industrial metal leaching process, utilizing an electrochemical three-electrode setup as required in SFC-ICP-MS measurements is not favorable. It would be cost-intensive and limit its applicability. On the other hand, two-electrode processes, which allow for the utilization of current control (galvanostatic) protocols, are considerably less complex. As demonstrated by our results using a current control measurement protocol reported in Fig. 3, it is feasible to selectively dissolve nearly all Ir from a bifunctional Pt-IrO_2/C catalyst (Fig. 4) by using such a current-based protocol. Moreover, this approach offers the advantage of being applicable in a simple two-electrode configuration, eliminating the need for a potentiostat.

3.5. *Proof-of-concept for Ir selective dissolution using application-relevant catalyst loading onto gas diffusion layers (GDLs)*

Finally, to provide proof of scalability of the presented approach, the bifunctional Pt-IrO_2/C nanocomposite was evaluated at an application-relevant loading of 400 $\mu g_{Pt\ +\ Ir}$ cm^{-2}, as outlined in Table 1. The

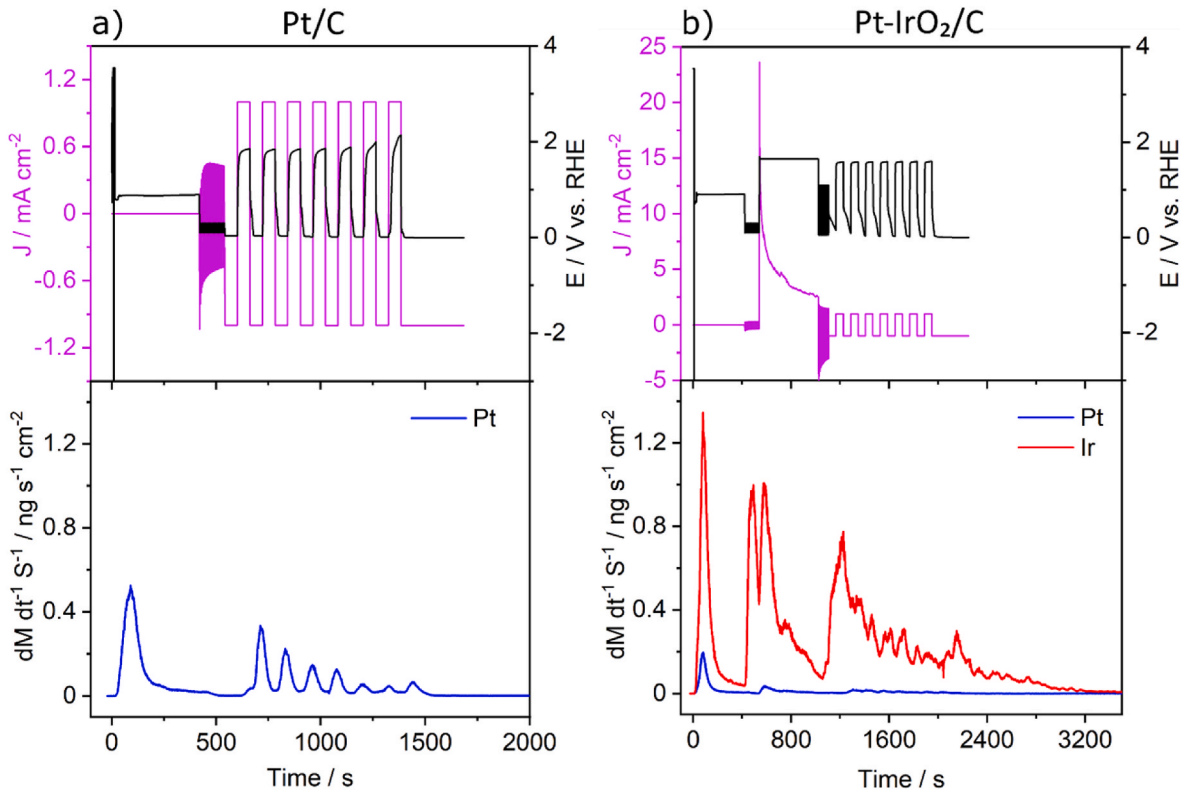

Fig. 3. Mass-specific metal dissolution rate of (a) 20 wt% Pt/C and (b) Pt (blue curves) and Ir (red curves) dissolution rates of 20 wt% Pt + 20 wt% Ir/C (Pt-IrO_2/C) nanocomposites. Applied treatment protocols and metal dissolution rates are plotted at the same time scale. The treatments were started with potential cycling between 0.10 and 0.30 V vs RHE at a scan rate of 100 mV s^{-1} for 30 cycles to reduce chemically formed native metal oxides, as indicated at ~400 s. This was followed by Ir electrochemically oxidation/activation to form bifunctional Pt-IrO_2/C nanocomposite by holding potential at 1.60 V vs RHE for 8 min, subsequently, sweeping potential between 0.05 and 1.10 V vs RHE at a scan rate of 500 mV s^{-1} for 20 cycles to stabilize the catalysts. Afterwards, switching to current control mode with current stepping between −1 mA cm^{-2} and 1 mA cm^{-2}, for each current the holding time is 60 s and 7 repeats in total. (For interpretation of the references to colour in this figure legend, the reader is referred to the Web version of this article.)

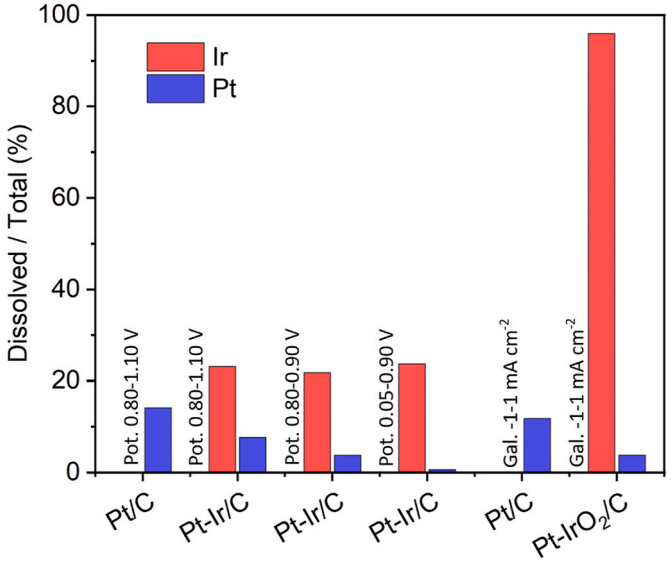

Fig. 4. Summary of total metal dissolution yields during measurements with different treatment protocols. Pt-Ir/C and Pt-IrO_2/C are used to differentiate the metallic and the activated Ir in the nanocomposites, respectively. Pt and Ir are introduced with the same weight ratio (20 wt%, respectively) in the nanocomposites. Pot.: potentiostatic, Gal.: galvanostatic. All potentials are relative to RHE.

experimental measurements were conducted in a straightforward jacketed-type electrochemical cell, and the extent of metal dissolution was assessed through ICP-MS analysis of the bulk electrolyte. Additionally, scanning electron microscopy coupled with energy dispersive X-ray spectroscopy (SEM-EDX) analysis was employed to examine the elemental changes in the catalyst layers before and after treatments, allowing for the determination of Ir dissolution selectivity.

It is seen that the choice of electrolyte noticeably influences the selectivity of Ir dissolution. Nevertheless, irrespective of the tested electrolyte media, selective Ir dissolution is observed when comparing the relative changes in surface elements using SEM-EDX analysis. Among the tested electrolytes, an H_2SO_4-based aqueous electrolyte yields the most favorable results, i.e. higher dissolution of Ir vs. Pt, which is likely resulted from a stronger interaction of HSO_4^- and SO_4^{2-} with surface Ir atoms [52] compared with, e.g., ClO_4^-. Methanol enhances the dissolution of Ir possibly via the facilitation of soluble IrO_4^{2-} formation [19]. In contrast, the metallic Pt surface remains relatively unaffected in the corresponding potential regime (Fig. S2d in supporting information). However, when comparing offline and online dissolution measurements, it becomes apparent that the selectivity in Ir dissolution is less pronounced in a jacket-type cell. For instance, in 1 M H_2SO_4, the maximum Ir dissolution normalized to its total loading is approximately 15 %. Several factors contribute to this observed difference. Firstly, there are variations in catalyst loadings on the working electrode. In the flow cell experiments, a typical catalyst loading of 4–10 $\mu g_{Cat.}$ cm_{geo}^{-2} was employed (see Table S2), whereas substantially higher loadings of 1000–1200 $\mu g_{Cat.}$ cm_{geo}^{-2} were used for the jacket-type cell measurements. Under these conditions, the resulting mass-normalized current densities are approx. 14 A g^{-1} in the jacket-type cell and approx. 140 A

Table 1
The calculated Ir/Pt weight ratio via SEM-EDX analysis before and after treatment, the change in Ir/Pt weight ratio and the dissolved Pt and Ir amount determined by ICP-MS during treatments to 20 wt% Pt + 20 wt% Ir/C (Pt-IrO_2/C). The averaged composition values in weight fraction are calculated from five different areas of catalyst layers (400 $\mu g_{Ir+Pt}\,cm^{-2}$), the calculation of Ir/Pt weight ratio change is based on the averaged wt. Ir/Pt values. All measurements are performed under 40 °C in air, and in a jacketed-type electrochemical cell. The error is the standard deviation of five independent measurements. 5 mL of electrolyte after treatment is taken out and diluted to an ideal concentration for ICP-MS measurements. ICP-MS measurements were not performed for 1 M H_2SO_4 + 0.5 M CH_3OH due to the potential harmful effects of CH_3OH on the ICP-MS equipment. BOT: before test, EOT: end of test.

Electrolyte	BOT wt. Ir/Pt	EOT wt. Ir/Pt	wt. Ir/Pt change (%)	Pt in electrolyte (μg)	Ir in electrolyte (μg)
1 M H_2SO_4	1.14 ± 0.07	0.44 ± 0.11	61.4	0.570	2.025
1 M $HClO_4$	1.16 ± 0.09	0.93 ± 0.06	19.8	0.105	0.255
1 M HNO_3	1.16 ± 0.12	0.58 ± 0.02	50.0	0.555	1.755
1 M H_2SO_4 + 0.5 M CH_3OH	1.19 ± 0.03	0.36 ± 0.03	69.7	–	–

g^{-1} in the SFC, representing a 10-fold higher mass-normalized current in the SFC, which results in an approx. 6.5-fold higher Ir dissolution (Table 1 and Fig. 4). Furthermore, in the jacketed-type cell, the redox processes of metal catalysts in the catalyst layer itself may be sufficient to maintain the current. In the simplest case the applied current 1 mA exclusively flows to Ir to drive its valence change between 4+ and 3+ during one current hold, which requires only about 2 μg Ir that is only one seventh of the Ir total mass (~14 μg) in catalyst layer. However, in the case of the SFC measurements, the catalyst loading is too low to sustain the current by redox processes. Instead, only the OER and hydrogen evolution reaction (HER) can maintain the applied current which requires substantially higher electrode potentials. As a consequence, the corresponding applied potentials differ. In the flow cell, the potentials varied between 0 and 2 V vs. RHE, while in the jacket-type cell, they were limited within the range of 0.70 and 1.20 V vs. RHE (Fig. S2). A third difference lies in the test environment. In a jacket-type cell, dissolved metals can redeposit onto the working electrode, whereas in a flow cell, they are flushed away. Furthermore, discrepancies in test temperatures and atmospheres may also contribute to the differences in selective Ir dissolution.

4. Conclusions and outlook

We presented the preparation and investigation of bifunctional Pt-Ir/C and Pt-IrO_2/C electrocatalysts using a nanocomposite concept to evaluate the viability of selective Ir electrochemical dissolution. The findings reveal that the treatment protocols employed significantly influence the dissolution rates of Pt and Ir. Comparatively, the reference catalyst, 20 wt% Pt/C, demonstrates the highest dissolution rate under both potential-based and current-based treatments when compared to the bifunctional nanocomposites. This suggests that the incorporation of Ir/IrO_2 in carbon-supported Pt-Ir/IrO_2 bifunctional catalysts effectively mitigates Pt degradation. However, it comes at the expense of substantial Ir dissolution. Thus, the inclusion of Ir/IrO_2 as an additional catalyst to Pt/C highlights the issue at hand but also presents a potential strategy for selectively recycling Ir.

Notably, the observation of Ir selective dissolution from Pt-Ir/IrO_2 bifunctional catalysts suggests that metallic Ir-based Pt-Ir/C catalysts can achieve selective Ir dissolution by lowering the potential to 0.05 V vs. RHE and subsequently switching back to 0.90 V vs. RHE, thereby minimizing Pt dissolution. Similarly, for Pt-IrO_2/C catalysts, selective Ir dissolution is achieved by employing a current-based protocol that is relevant for practical application and switching between approximately 0 and 2 V vs. RHE, while maintaining Pt dissolution at a minimum.

Remarkably, nearly all (96 %) Ir can be selectively dissolved while minimizing Pt dissolution. Furthermore, the concept is demonstrated using catalyst films with realistic catalyst loading on a carbon-based GDL. Therefore, these results indicate that electrochemically selective Ir recycling, based on its preferential dissolution, could be a promising strategy to address the issue of Ir scarcity further to achieve a sustainable implementation of PEMWE technology based on PGM materials.

While the various successful proof-of-concept demonstrations reported here on the selective dissolution of Ir, the possibility of using a 2-electrode setup, and the viability of the process at application-relevant catalyst loadings are promising, there is still room for optimization before the approach can be fully implemented at a large scale. Future areas of research include, for example, a deeper understanding of the Ir species involved, the Ir electrochemical dissolution mechanism, recovery efficiency, and/or post-recovery activity evaluation. Nevertheless, the results presented provide a solid ground for developing new strategies for Ir recovery from bifunctional catalyst layers in PEMWE.

CRediT authorship contribution statement

Jia Du: Writing – original draft, Visualization, Validation, Investigation, Data curation. **Matej Zlatar:** Writing – review & editing, Investigation, Formal analysis, Data curation. **Damin Zhang:** Writing – review & editing, Investigation, Formal analysis. **Daniel Escalera-López:** Writing – review & editing, Investigation, Formal analysis, Data curation. **Jonathan Quinson:** Writing – review & editing, Validation, Formal analysis. **Serhiy Cherevko:** Writing – review & editing, Validation, Supervision, Funding acquisition, Conceptualization. **Matthias Arenz:** Writing – review & editing, Supervision, Funding acquisition, Conceptualization.

Declaration of Generative AI and AI-assisted technologies in the writing process

During the preparation of this work the authors used ChatGPT to review individual sections of the manuscript to improve the readability and style of the text. After using ChatGPT, the authors reviewed and edited the content as needed and take full responsibility for the content of the publication. ChatGPT was not used to suggest, select nor include any of the references reported.

Declaration of competing interest

The authors declare that they have no known competing financial interests or personal relationships that could have appeared to influence the work reported in this paper.

Acknowledgements

This Project has received funding from the European Union's Horizon 2020 Research and Innovation program under grant agreement No. 861960 ("Recycalyse" project) and the Swiss National Science Foundation (SNSF) via the project No. 200021_184742. Furthermore, work was also supported by Deutsche Forschungsgemeinschaft (DFG) within the grant CH 1763/4-1.

Appendix A. Supplementary data

Supplementary data to this article can be found online at https://doi.org/10.1016/j.jpowsour.2025.238224.

Data availability

Data will be made available on request.

References

[1] C. Minke, M. Suermann, B. Bensmann, R. Hanke-Rauschenbach, Is iridium demand a potential bottleneck in the realization of large-scale PEM water electrolysis? Int. J. Hydrogen Energy 46 (2021) 23581–23590, https://doi.org/10.1016/j.ijhydene.2021.04.174.

[2] C. Van Pham, D. Escalera-López, K. Mayrhofer, S. Cherevko, S. Thiele, Essentials of high performance water electrolyzers – from catalyst layer materials to electrode engineering, Adv. Energy Mater. 11 (2021) 2101998, https://doi.org/10.1002/aenm.202101998.

[3] U. Babic, M. Suermann, F.N. Büchi, L. Gubler, T.J. Schmidt, Critical Review—Identifying critical gaps for polymer electrolyte water electrolysis development, J. Electrochem. Soc. 164 (2017) F387–F399, https://doi.org/10.1149/2.1441704jes.

[4] G. Gao, Z. Sun, X. Chen, G. Zhu, B. Sun, Y. Yamauchi, S. Liu, Recent advances in Ru/Ir-based electrocatalysts for acidic oxygen evolution reaction, Appl. Catal., B 343 (2024) 123584, https://doi.org/10.1016/j.apcatb.2023.123584.

[5] Y. Liu, Q. Song, T. Xu, Q. Kong, G. He, H. Sun, H. Li, Z. Yuan, X. Ma, X. Su, X. ping Dai, Q. Zhang, Z.X. Li, Y.C. Wei, X. Zhang, Novel large-scale integrated non-precious metal electrodes for efficient and stable oxygen evolution reaction at high current density in 2.5 kW anion exchange membrane water electrolysis, Appl. Catal., B 363 (2025) 124811, https://doi.org/10.1016/j.apcatb.2024.124811.

[6] W. Bernhart, S. Riederle, M. Yoon, W.G. Aulbur, Fuel cells — a realistic alternative for zero emission? Auto Tech Review 3 (2014) 18–23, https://doi.org/10.1365/s40112-014-0568-z.

[7] Y. Feng, Y. Xie, Y. Yu, Y. Chen, Q. Liu, H. Bao, F. Luo, S. Pan, Z. Yang, Electronic metal-support interaction induces hydrogen spillover and platinum utilization in hydrogen evolution reaction, Angewandte Chemie - International Edition 64 (2025) e202413417, https://doi.org/10.1002/anie.202413417.

[8] C. Zhang, Q. Zhang, Y. Hu, H. Hu, J. Yang, C. Yang, Y. Zhu, Z. Tu, D. Wang, N-doped carbon confined ternary Pt2NiCo intermetallics for efficient oxygen reduction reaction, Chin. Chem. Lett. 36 (2025) 110429, https://doi.org/10.1016/j.cclet.2024.110429.

[9] Q. Li, Y. Feng, Y. Xie, Q. Xu, Y. Li, Y. Yu, F. Luo, Z. Yang, MOF derived RuO2/V2O5 nanoneedles for robust and stable water oxidation in acid, Chin. Chem. Lett. 36 (2025) 111074, https://doi.org/10.1016/j.cclet.2025.111074.

[10] R.E. Smalley, Future global energy prosperity: the terawatt challenge, MRS Bull. 30 (2005) 412–417, https://doi.org/10.1557/mrs2005.124.

[11] M. Clapp, C.M. Zalitis, M. Ryan, Perspectives on current and future iridium demand and iridium oxide catalysts for PEM water electrolysis, Catal. Today 420 (2023) 114140, https://doi.org/10.1016/j.cattod.2023.114140.

[12] C. Saguru, S. Ndlovu, D. Moropeng, A review of recent studies into hydrometallurgical methods for recovering PGMs from used catalytic converters, Hydrometallurgy 182 (2018) 44–56, https://doi.org/10.1016/j.hydromet.2018.10.012.

[13] L. Predzymirska, T. Barreiros, A. Thiere, A. Weigelt, D. Vogt, M. Stelter, A. Charitos, Recycling Strategy for the Extraction of Pgms from Spent PEM Electrodes, 2021.

[14] N. Hodnik, C. Baldizzone, G. Polymeros, S. Geiger, J.P. Grote, S. Cherevko, A. Mingers, A. Zeradjanin, K.J.J. Mayrhofer, Platinum recycling going green via induced surface potential alteration enabling fast and efficient dissolution, Nat. Commun. 7 (2016) 13164, https://doi.org/10.1038/ncomms13164.

[15] M.K. Jha, J.C. Lee, M.S. Kim, J. Jeong, B.S. Kim, V. Kumar, Hydrometallurgical recovery/recycling of platinum by the leaching of spent catalysts: a review, Hydrometallurgy 133 (2013) 23–32, https://doi.org/10.1016/j.hydromet.2012.11.012.

[16] G. Schreier, C. Edtmaier, Separation of Ir, Pd and Rh from secondary Pt scrap by precipitation and calcination, n.d. www.elsevier.com/locate/hydromet.

[17] S. Ivlev, P. Woidy, F. Kraus, I. Gerin, R. Ostvald, Tetrafluorobromates for urban mining of noble metals: a case study on iridium metal, Eur. J. Inorg. Chem. (2013) 4984–4987, https://doi.org/10.1002/ejic.201300618.

[18] S. Turnbull, D. Clauss, V. Martin, J.P. Magnin, L. Dubau, F. Maillard, An aqua regia-free chemical recovery and reprecipitation of Ir from IrOx catalysts: optimisation of the extraction efficiency using surface response methodology, RSC Sustain. 3 (2025) 1741–1750, https://doi.org/10.1039/d5su00038f.

[19] L. Moriau, K. Stojanovski, P. Jovanovič, D. Escalera-López, S. Cherevko, N. Hodnik, Towards electrochemical iridium recycling in acidic media: effect of the presence of organic molecules and chloride ions, RSC Adv. 13 (2023) 7980–7987, https://doi.org/10.1039/d2ra07142h.

[20] J. Du, J. Quinson, D. Zhang, F. Bizzotto, A. Zana, M. Arenz, Bifunctional Pt-IrO2Catalysts for the oxygen evolution and oxygen reduction reactions: alloy nanoparticles versus nanocomposite catalysts, ACS Catal. 11 (2021) 820–828, https://doi.org/10.1021/acscatal.0c03867.

[21] J. Du, J. Quinson, A. Zana, M. Arenz, Elucidating Pt-Based nanocomposite catalysts for the oxygen reduction reaction in rotating disk electrode and gas diffusion electrode measurements, ACS Catal. 11 (2021) 7584–7594, https://doi.org/10.1021/acscatal.1c01496.

[22] G.C. da Silva, K.J.J. Mayrhofer, E.A. Ticianelli, S. Cherevko, The degradation of Pt/IrOx oxygen bifunctional catalysts, Electrochim. Acta 308 (2019) 400–409, https://doi.org/10.1016/j.electacta.2019.04.017.

[23] G.C. da Silva, K.J.J. Mayrhofer, E.A. Ticianelli, S. Cherevko, Dissolution stability: the major challenge in the regenerative fuel cells bifunctional catalysis, J. Electrochem. Soc. 165 (2018) F1376–F1384, https://doi.org/10.1149/2.1201816jes.

[24] V. Shkirskiy, F.D. Speck, N. Kulyk, S. Cherevko, On the time resolution of electrochemical scanning flow cell coupled to downstream analysis, J. Electrochem. Soc. 166 (2019) H866–H870, https://doi.org/10.1149/2.1401915jes.

[25] M. Fathi Tovini, A.M. Damjanovic, H.A. El-Sayed, J. Speder, C. Eickes, J.-P. Suchsland, A. Ghielmi, H.A. Gasteiger, Degradation mechanism of an IrO2 anode Co-Catalyst for cell voltage reversal mitigation under transient operation conditions of a PEM fuel cell, J. Electrochem. Soc. 168 (2021) 064521, https://doi.org/10.1149/1945-7111/ac0d39.

[26] J. Quinson, M. Inaba, S. Neumann, A.A. Swane, J. Bucher, S.B. Simonsen, L. Theil Kuhn, J.J.K. Kirkensgaard, K.M. Jensen, M. Oezaslan, S. Kunz, M. Arenz, Investigating particle size effects in catalysis by applying a size-controlled and surfactant-free synthesis of colloidal nanoparticles in alkaline ethylene glycol: case Study of the oxygen reduction reaction on Pt, ACS Catal. 8 (2018) 6627–6635, https://doi.org/10.1021/acscatal.8b00694.

[27] V. Yarlagadda, S.E. McKinney, C.L. Keary, L. Thompson, B. Zulevi, A. Kongkanand, Preparation of PEMFC electrodes from milligram-amounts of catalyst powder, J. Electrochem. Soc. 164 (2017) F845–F849, https://doi.org/10.1149/2.1461707jes.

[28] S. Cherevko, S. Geiger, O. Kasian, A. Mingers, K.J.J. Mayrhofer, Oxygen evolution activity and stability of iridium in acidic media. Part 1. - metallic iridium, J. Electroanal. Chem. 773 (2016) 69–78, https://doi.org/10.1016/j.jelechem.2016.04.033.

[29] S. Cherevko, S. Geiger, O. Kasian, A. Mingers, K.J.J. Mayrhofer, Oxygen evolution activity and stability of iridium in acidic media. Part 2. - electrochemically grown hydrous iridium oxide, J. Electroanal. Chem. 774 (2016) 102–110, https://doi.org/10.1016/j.jelechem.2016.05.015.

[30] S. Cherevko, Electrochemical dissolution of noble metals native oxides, J. Electroanal. Chem. 787 (2017) 11–13, https://doi.org/10.1016/j.jelechem.2017.01.029.

[31] S. Cherevko, Electrochemical dissolution of noble metals, Encyclopedia of Interfacial Chemistry: surface Science and electrochemistry, 68–75, https://doi.org/10.1016/B978-0-12-409547-2.13569-3, 2018.

[32] S. Cherevko, A.R. Zeradjanin, A.A. Topalov, N. Kulyk, I. Katsounaros, K.J. J. Mayrhofer, Dissolution of noble metals during oxygen evolution in acidic media, ChemCatChem 6 (2014) 2219–2223, https://doi.org/10.1002/cctc.201402194.

[33] M. Zlatar, D. Escalera-López, M.G. Rodríguez, T. Hrbek, C. Götz, R. Mary Joy, A. Savan, H.P. Tran, H.N. Nong, P. Pobedinskas, V. Briega-Martos, A. Hutzler, T. Böhm, K. Haenen, A. Ludwig, I. Khalakhan, P. Strasser, S. Cherevko, Standardizing OER electrocatalyst benchmarking in aqueous electrolytes: comprehensive guidelines for accelerated stress tests and backing electrodes, ACS Catal. 13 (2023) 15375–15392, https://doi.org/10.1021/acscatal.3c03880.

[34] A. Taniguchi, T. Akita, K. Yasuda, Y. Miyazaki, Analysis of electrocatalyst degradation in PEMFC caused by cell reversal during fuel starvation, J. Power Sources 130 (2004) 42–49, https://doi.org/10.1016/j.jpowsour.2003.12.035.

[35] B.K. Hong, P. Mandal, J.G. Oh, S. Litster, On the impact of water activity on reversal tolerant fuel cell anode performance and durability, J. Power Sources 328 (2016) 280–288, https://doi.org/10.1016/j.jpowsour.2016.07.002.

[36] Y. Yu, H. Li, H. Wang, X.Z. Yuan, G. Wang, M. Pan, A review on performance degradation of proton exchange membrane fuel cells during startup and shutdown processes: causes, consequences, and mitigation strategies, J. Power Sources 205 (2012) 10–23, https://doi.org/10.1016/j.jpowsour.2012.01.059.

[37] F. Bizzotto, J. Quinson, J. Schröder, A. Zana, M. Arenz, Surfactant-free colloidal strategies for highly dispersed and active supported IrO2 catalysts: synthesis and performance evaluation for the oxygen evolution reaction, J. Catal. (2021) 54–62, https://doi.org/10.1016/J.JCAT.2021.07.004.

[38] F. Bizzotto, J. Quinson, A. Zana, J.J.K. Kirkensgaard, A. Dworzak, M. Oezaslan, M. Arenz, Ir nanoparticles with ultrahigh dispersion as oxygen evolution reaction (OER) catalysts: synthesis and activity benchmarking, Catal. Sci. Technol. 9 (2019) 6345–6356, https://doi.org/10.1039/c9cy01728c.

[39] M. Zlatar, D. Escalera-López, C. Simon, V. Briega-Martos, K. Stojanovski, S. Cherevko, pH dependence of noble metals dissolution: iridium, Electrochim. Acta 513 (2025) 145450, https://doi.org/10.1016/j.electacta.2024.145450.

[40] S. Cherevko, G.P. Keeley, S. Geiger, A.R. Zeradjanin, N. Hodnik, N. Kulyk, K.J. J. Mayrhofer, Dissolution of platinum in the operational range of fuel cells, Chemelectrochem 2 (2015) 1471–1478, https://doi.org/10.1002/celc.201500098.

[41] A.A. Topalov, S. Cherevko, A.R. Zeradjanin, J.C. Meier, I. Katsounaros, K.J. J. Mayrhofer, Towards a comprehensive understanding of platinum dissolution in acidic media, Chem. Sci. 5 (2013) 631–638, https://doi.org/10.1039/c3sc52411f.

[42] A.A. Topalov, I. Katsounaros, M. Auinger, S. Cherevko, J.C. Meier, S.O. Klemm, K. J.J. Mayrhofer, Dissolution of platinum: limits for the deployment of electrochemical energy conversion? Angew. Chem. Int. Ed. 51 (2012) 12613–12615, https://doi.org/10.1002/anie.201207256.

[43] S. Cherevko, A.R. Zeradjanin, G.P. Keeley, K.J.J. Mayrhofer, A comparative study on gold and platinum dissolution in acidic and alkaline media, J. Electrochem. Soc. 161 (2014) H822–H830, https://doi.org/10.1149/2.0881412jes.

[44] K.J. Vetter, J.W. Schultze, The kinetics of the electrochemical formation and reduction of monomolecular oxide layers on platinum in 0.5 M H2SO4: part II. Galvanostatic pulse measurements and the model of oxide growth, J. Electroanal. Chem. Interfacial Electrochem. 34 (1972) 141–158, https://doi.org/10.1016/S0022-0728(72)80510-2.

[45] B.E. Conway, Electrochemical oxide film formation at noble metals as a surface-chemical process, Prog. Surf. Sci. 49 (1995) 331–452, https://doi.org/10.1016/0079-6816(95)00040-6.
[46] H. Angerstein-Kozlowska, B.E. Conway, W.B.A. Sharp, The real condition of electrochemically oxidized platinum surfaces: part I. Resolution of component processes, J. Electroanal. Chem. Interfacial Electrochem. 43 (1973) 9–36, https://doi.org/10.1016/S0022-0728(73)80307-9.
[47] B. V Tilak, B.E. Conway, H. Angerstein-Kozlowska, The real condition of oxidized pt electrodes: part III. Kinetic theory of formation and reduction of surface oxides, J. Electroanal. Chem. Interfacial Electrochem. 48 (1973) 1–23, https://doi.org/10.1016/S0022-0728(73)80290-6.
[48] S. Cherevko, Electrochemical dissolution of noble metals, in: K. Wandelt (Ed.), Encyclopedia of Interfacial Chemistry, Elsevier, Oxford, 2018, pp. 68–75, https://doi.org/10.1016/B978-0-12-409547-2.13569-3.
[49] O. Kasian, J.-P. Grote, S. Geiger, S. Cherevko, K.J.J. Mayrhofer, The common intermediates of oxygen evolution and dissolution reactions during water electrolysis on iridium, Angew. Chem. Int. Ed. 57 (2018) 2488–2491, https://doi.org/10.1002/anie.201709652.
[50] I.C. Man, H.-Y. Su, F. Calle-Vallejo, H.A. Hansen, J.I. Martínez, N.G. Inoglu, J. Kitchin, T.F. Jaramillo, J.K. Nørskov, J. Rossmeisl, Universality in oxygen evolution electrocatalysis on oxide surfaces, ChemCatChem 3 (2011) 1159–1165, https://doi.org/10.1002/cctc.201000397.
[51] B. Huang, Y. Zhao, Iridium-based electrocatalysts toward sustainable energy conversion, EcoMat 4 (2022) e12176, https://doi.org/10.1002/eom2.12176.
[52] J.A. Arminio-Ravelo, A.W. Jensen, K.D. Jensen, J. Quinson, M. Escudero-Escribano, Electrolyte effects on the electrocatalytic performance of iridium-based nanoparticles for oxygen evolution in rotating disc electrodes, ChemPhysChem 20 (2019) 2956–2963, https://doi.org/10.1002/cphc.201900902.